Comparison of Headspace and Gas-Stripping Techniques for Measuring the Air−Water Partititioning of Normal Alkanols (C4 to C10): Effect of Temperature, Chain Length, and Adsorption to the Water Surface

Ying Duan Lei,[†,‡,§] Chubashini Shunthirasingham,[‡,§] and Frank Wania*[,§]

Department of Chemistry, Department of Chemical Engineering and Applied Chemistry, and Department of Physical and Environmental Sciences, University of Toronto at Scarborough, 1265 Military Trail, Toronto, Ontario, Canada M1C 1A4

The air−water partition coefficients K_{AW}^{C} of normal alkanols (C4 to C10) were determined as a function of temperature using both the phase ratio variation headspace (PRV−HS) method and the inert gas-stripping (IGS) method. Whereas the results of the PRV−HS experiments conducted at (50 to 90) °C were in good agreement with previous measurements for butan-1-ol, penta-1-ol, and heptan-1-ol, the K_{AW}^{C} values obtained from the IGS experiments performed at (25, 31, 51, and 69) °C were too high when compared to the PRV−HS results, literature values, and predictions based on vapor pressure and water solubility. For the short-chain alkanols and for the K_{AW}^{C} at higher temperatures, this discrepancy is likely due to evaporation from the stripping vessel. For the longer chain alkanols at lower temperatures, it is additionally due to adsorption to the air−water interface of the gas bubbles. The magnitude and dependence of the latter artifact on chain length and temperature is consistent with predictions based on interfacial adsorption coefficients (K_{IA}) and bubble radius. The evaporation effect leads to an overestimation of the temperature dependence of air−water partitioning, whereas the surface adsorption effect can cause the opposite for substances with strong adsorption to the water surface. The validity of previously published air−water partitioning data that have been generated for substances with relatively high K_{IA} (>10 mm) using the IGS method should be re-evaluated.

Introduction

The equilibrium partition coefficient of a compound between air and water is the ratio of its abundance in the gas phase and the aqueous dissolved phase at equilibrium. If the abundance in both air and water is expressed in molar concentrations, C_A and C_W in mol·m^{-3}, this ratio is a dimensionless parameter, K_{AW}^{C}:

$$K_{AW}^{C} = C_A/C_W \quad (1)$$

If the abundance of the compound in air is expressed in terms of partial pressure, the ratio, K_{AW}^{P}, has units of Pa·m^3·mol^{-1}. For neutral compounds at dilute solution in pure water, K_{AW}^{C} and K_{AW}^{P} are also referred to as Henry's law constant.[1] K_{AW}^{C} is of utmost importance in a variety of fields. In particular, it is indispensable when trying to understand, predict, and simulate the environmental behavior of organic contaminants: the K_{AW}^{C} of a compound determines the exchange between atmosphere and water bodies, including lakes, rivers, and oceans; it controls the extent of precipitation scavenging; and its magnitude determines whether the kinetic control of diffusive air−water exchange is on the air or water side.[1]

A popular technique for measuring the air−water partition coefficient is the inert gas-stripping (IGS) method, in which an inert gas is used to sparge an organic solute from an aqueous solution. In the original version of the technique, described by Leroi et al.,[2] the decrease of the solute concentration in the gas phase is monitored by gas chromatographic analysis. Mackay et al.[3] showed that for hydrophobic chemicals it is often preferable to observe the decrease of the aqueous concentration. In either case, it is possible to derive the air−water partition coefficient from the rate of concentration decline. An advantage of the technique is that only relative and not absolute concentrations need to be established, eliminating the need for calibration and quantification. Also, in contrast to techniques that rely on the quantification of concentrations in air and water to derive an air−water partition coefficient, only one phase (i.e., either air or water) needs to be sampled and analyzed. Precision is further aided by using multiple data points in a linear regression in the derivation of a single K_{AW}^{C} value. By employing a flow-through cell and suitable detection techniques, continuous monitoring of the aqueous concentration decline has been achieved.[4] Hovorka and Dohnal[5] have used the method extensively for a variety of volatile substances and have derived correction factors to yield highly accurate measurements.

In the past 30 years, the technique has been used to measure the air−water partitioning of a wide variety of chemicals, including chlorobenzenes,[6,7] polycyclic aromatic hydrocarbons,[4,6−10] polychlorinated biphenyls,[6,11−13] polybrominated diphenyl ethers,[13,14] carbazole,[15] hexachlorocyclohexanes,[16,17] toxaphene,[18] and other organochlorine pesticides.[19,20] The technique has been used to determine air−water partitioning as a function of temperature and water salinity.[16,19]

For substances with a relatively low K_{AW}^{C}, the rate of concentration decline can be very slow, necessitating very long sparging times to observe measurable concentration declines. This has prompted the modification of the technique, whereby air and water concentrations are determined and the K_{AW}^{C} is

* Corresponding author. E-mail: frank.wania@utoronto.ca.
† Department of Chemistry.
‡ Department of Chemical Engineering and Applied Chemistry.
§ Department of Physical and Environmental Sciences.

10.1021/je060344q CCC: $37.00
Published on Web 11/23/2006

calculated from their ratio.[12,13] In that case the objective of using a dynamic stripping technique is to equilibrate large volumes of air with relatively small volumes of water to achieve quantifiable amounts in the gas phase. This modification however also negates some of the main advantages of the original method mentioned above.

Recently, Goss et al.[21] suggested that the IGS technique may suffer from systematic artifacts when applied to chemicals that experience appreciable adsorption to the water surface. When the gas bubbles stripping the aqueous solution burst at the top of the water column, a fraction of the chemical sorbed to the bubble surface is likely to be transferred to the gas phase. This may result in apparent air−water partition coefficients that are higher than expected based on bulk air−water partitioning only. Goss et al.[21] used this artifact to explain discrepancies between the K_{AW}^{P} values for highly chlorinated PCBs determined with the IGS technique[12] and those measured by other techniques that are not susceptible to artefacts caused by adsorption to the water surface. Baker et al.[22] have challenged that explanation, and until now there is no agreement as to the magnitude or even as to the occurrence of such an artifact.

The objective of the current study was to investigate whether surface adsorption can bias the result of air−water partition coefficient measurements with the IGS method. The approach taken was to determine the K_{AW}^{C} for a series of organic chemicals showing highly variable adsorption to the water surface, with both the IGS technique and the variable phase ratio headspace technique, a method that should be much less susceptible to artifacts caused by adsorption to the water surface. Normal alkanols from butan-1-ol to decan-1-ol were considered ideal candidates for the study because they show a large increase in adsorption to the water surface with increasing chain length. Because the artifact is predicted to be more pronounced at low temperatures,[21] we further measured K_{AW}^{C} of these alkanols as a function of temperature with both methods. Sagebiel et al.[23] has previously compared headspace and IGS methods for Henry's law constant measurements, but not with the intention to investigate the role of adsorption to the water surface.

Theory

Inert Gas-Stripping Method. In the IGS method, the decline of the concentration of an organic compound in aqueous solution $C(t)$ is recorded as a function of time t (in min) while it is sparged from a column of water by an inert gas. If equilibrium between the water in the sparging column and the gas phase in the air bubbles is achieved, a plot of the logarithm of the water concentrations, normalized to the initial water concentration C_0 at time 0 against time should yield a straight line:[3]

$$\ln(C(t)/C_0) = -(K_{AW}^{C}G/V)t \quad (2)$$

where G is the gas sparging rate (in $m^3 \cdot min^{-1}$) and V is the volume of water in the sparging column (in m^3). If the measured instrument signal A is proportional to the solute concentration C over the entire concentration range encountered during the experiment, no quantification of absolute water concentrations is required, and $\ln(C/C_0)$ in eq 2 can simply be replaced with $\ln(A/A_0)$. The gas stream is usually saturated with water prior to sparging to avoid the loss of water from the sparging column by evaporation. However, the repeated taking of aliquot for quantification of the water concentration typically leads to a gradual loss of water from the sparging column. It is thus advisable to measure or calculate the volume of water over the time course of the experiment and plot $\ln(A/A_0)$ against $t/V(t)$:

$$\ln(A(t)/A_0) = -(K_{AW}^{C}G)t/V(t) \quad (3)$$

K_{AW}^{C} is then simply obtained by dividing the slope of this linear relationship by the gas flow rate.

The above derivation assumes that only chemical partitioning into the gas phase of the bubbles is lost from the water phase upon bursting of the bubbles at the top of the water column. Organic chemicals adsorb to the water surface,[24,25] a process often described quantitatively using adsorption coefficients (or interfacial partitioning coefficients) between the water surface and the gas phase K_{IA} or between the water surface and the dissolved water phase K_{IW}, both expressed in units of length [$m = (mol \cdot m^{-2})/(mol \cdot m^{-3})$]. Upon bursting of a gas bubble the surface of that bubble disappears very rapidly, forcing the chemical adsorbed to the bubble surface to either re-dissolve in the aqueous phase or to enter the gas phase. The transfer to the gas phase does not only occur in aerosol form. At the moment of bubble bursting, the fugacity on the rapidly shrinking surface is expected to spike, providing a driving force for chemical transfer in vapor form. If transfer to the gas phase occurs, the sparging of chemical from the water column during a gas-stripping experiment occurs faster than what would be expected if only bulk phase partitioning between dissolved and gas phase is taken into account. In other words, a IGS experiment may yield erroneously large K_{AW}^{C} values for substances that adsorb appreciably to the water surface.

During IGS the loss of chemical is due to the chemical partitioning from the aqueous phase into the gas phase of the bubble (controlled by K_{AW}^{C}) and due to chemical adsorbing from the aqueous phase to the surface of the bubble (controlled by K_{IW}). The contribution of the latter relative to the former has to be weighted by the surface to volume ratio of the bubble and corrected for the fraction f_{TGB} of the chemical amount on the surface that is transferred to the gas phase upon bursting of the bubbles. The surface to volume ratio of a spherical bubble is $(4\pi r^2)/(4\pi r^3/3)$ or $3/r$, where r is the radius of the bubble. Therefore, a IGS experiment yields an apparent air−water partition coefficient of

$$K_{AW}^{C_{app}} = K_{AW}^{C} + K_{IW} f_{TGB} 3/r \quad (4)$$

Replacing K_{IW} with $K_{IA} \cdot K_{AW}^{C}$, eq 4 can also be written as

$$K_{AW}^{C_{app}} = K_{AW}^{C}(1 + f_{TGB}K_{IA} 3/r) = K_{AW}^{C} \cdot EF \quad (5)$$

The term $(1 + f_{TGB}K_{IA} 3/r)$ can be defined as the enhancement factor (EF) quantifying the extent to which the measured apparent $K_{AW}^{C_{app}}$ is higher than the real K_{AW}^{C}. From eq 5, we can deduce that the potential error in K_{AW}^{C} is larger for chemicals that sorb strongly to the water surface (those with high K_{IA} values) and in experiments with small bubble sizes (small r). We note that a small bubble size is typically desired in IGS experiments, as it speeds up the mass transfer from dissolved to gas phase and thus helps to ensure that equilibrium is being established. However, Hoff et al.[25] had noted that "when making measurements of air−water partition coefficient by stripping techniques, it is unwise to create bubbles which are so small that interfacial partitioning becomes appreciable".

Phase Ratio Variation Headspace Method. In the phase ratio variation headspace (PRV−HS) method, variable volumes of the same aqueous solution of an analyte are equilibrated with the gas phase in closed vials of the same total volume.[26] Each vial experiences a different phase ratio β, which is linearly related to the reciprocal of the headspace concentration. The

equilibrium partition coefficient between water and the gas phase can be derived from the slope and intercept of this linear relationship. A detailed description of the theory underlying the phase ratio variation method can be found elsewhere.[26,27] Briefly, the concentration C_A of a solute in the vial headspace at equilibrium is

$$C_A = C_{W0}/(1/K^C_{AW} + \beta) \quad (6)$$

where C_{W0} is the original molar concentration of the solute in water and β is the ratio of the volumes of the headspace and the aqueous phase. If the measured instrument signal A is again linearly related to the equilibrium concentration of the analyte in the headspace, we can replace C_A with A. Taking reciprocals of both sides of eq 6, we obtain

$$1/A = 1/(K^C_{AW}C_{W0}) + 1/C_{W0}\beta \quad (7)$$

The phase ratio β is varied (by filling different volumes of the same aqueous solution into a number of equally sized vials), A is measured, and K^C_{AW} and C_{W0} are constants. A plot of reciprocal instrument signal against the phase ratio should thus be linear, and the ratio of the slope $1/C_{W0}$ and the intercept $1/(K^C_{AW}C_{W0})$ of such a plot yields the K^C_{AW}. Note that neither C_A nor C_{W0} need to be known or quantified. This implies that the PRV−HS method shares several advantages with the IGS technique: Measurements of concentrations in only one of the two involved phases is required. The IGS technique relies on measurements of the solute in air or water, whereas the PRV−HS method measures the chemicals in the gas phase. Because the methods rely on relative rather than absolute concentration measurements, no calibration or absolute quantification is required; in both methods, the measured instrument signal A can be directly used in the determination of the partition coefficient. Finally, in either case, the partition coefficient is derived from the linear regression of multiple measurements.

We should note that a chemical can also adsorb to the air−water interface in the headspace vial. If we consider that possibility, eq 7 should read:

$$1/A = 1/(K^C_{AW}C_{W0}) + 1/C_{W0}(\beta + K_{IA}\cdot S/V_W) = 1/(K^C_{AW}C_{W0}) + 1/C_{W0}((V_A + K_{IA}\cdot S)/V_W) \quad (8)$$

where S is the surface area of the air−water interface and V_A and V_W are the volumes of headspace and water phase in the vial, respectively. V_A in our experiments is between $(2.03\cdot10^{-5}$ and $2.22\cdot10^{-5})$ m^3, and the surface area S less than $7\cdot10^{-4}$ m^2. The highest estimated K_{IA} values for the conditions of our experiments are 0.0004 m for decan-1-ol at 60 °C and 0.0007 m for nona-1-ol at 50 °C. The largest error in phase ratio β that we make when using eq 7 is thus less than 2 %. However, for chemicals with higher K_{IA} than the long-chain alkanols or for experiments at lower temperatures, even the PRV−HS method is suseptible to artefacts caused by adsorption to the air−water interface.

Experimental Section

Inert Gas-Stripping Method. We used the gas-stripping apparatus described in detail in the papers by Mackay et al.[3] and Shiu and Mackay.[7] It consists of two concentric glass cylinders, with the inner cylinder (6 cm i.d.) containing the solution being stripped (water column height of 30 cm) and the outer cylinder being a thermostatted water jacket. The stripping gas is introduced into the bottom of the inner cylinder with the help of a sintered glass disk, which causes the gas stream to disperse into large numbers of small air bubbles rising to the top of the water column. A stopcock at the bottom of the apparatus allows for easy sampling of water aliquots.

An aqueous solution of the alkanols was prepared by first dissolving 10 μL each of butan-1-ol, pentan-1-ol, hexan-1-ol, heptan-1-ol, octan-1-ol, nonan-1-ol, and decan-1-ol in 1 mL of methanol. This solution was diluted into 1 L of Milli-Q water, which was stirred overnight with a stir bar in a stoppered Erlenmeyer flask. A total of 500 mL of this solution, containing 8 mg·L^{-1} of each alkanol, was transferred into the gas-stripping column, which was maintained at a constant temperature with the help of the water jacket and a circulating bath. The water was allowed to sit in the thermostatted column overnight prior to gas stripping. The stripping gas was nitrogen, humidified by passing it through a water-filled wash bottle. The flow rate of the stripping gas was determined at regular intervals with a bubble flowmeter at the outflow of the stripping column. Most experiments were conducted at a nominal flow rate of 200 ± 2 mL·min^{-1}, but some experiments were conducted at lower flow rates of (50 and 100) mL·min^{-1}, respectively. The nominal flow rates measured at room temperature were adjusted to the temperature of the stripping column using the ideal gas law. The bubble size increased with flow rate (Figure 1). The average radius of the bubbles at different flow rates was determined from counting different size classes of bubbles in multiple segments of digital photographs of the stripping column (Figure 1). They were (0.882 ± 0.005, 1.105 ± 0.003, and 1.464 ± 0.007) mm for nominal flow rates of (50, 100, and 200) mL·min^{-1}, respectively.

In total, six IGS experiments were performed: Experiments at (25, 31, 51, and 69) °C were conducted with a nominal gas flow rate of 200 mL·min^{-1}. Additionally, experiments were performed at 25 °C and 100 mL·min^{-1} and at 51 °C and 50 mL·min^{-1}. As the alkanols were being stripped from the water solutions at different rates, aliquots of water were taken at short intervals (15 to 30 min) during the first few hours of the experiments and much longer intervals afterward. The overall length of the experiments varied according to the temperature of the solution (being longer at lower temperatures) but generally lasted no longer than a few days.

During a sampling event, the gas flow was stopped briefly to drain 1.5 mL of water into a vial. A total of 500 μL of this solution was micropipetted into two 22.3 mL headspace vials and capped immediately. The vials were analyzed by headspace analysis using a Perkin-Elmer HS-40XL automatic headspace sampler connected to a Perkin-Elmer Auto System XL gas chromatograph. The headspace vials were thermostatted at 70 °C for 60 min. The headspace injection needle was at 135 °C and the transfer line at 140 °C. Pressurization lasted 1 min and injection 0.06 min. The alkanols were separated on a DB-Wax capillary column (0.25 mm i.d. × 30 m long, 0.25 μm film thickness, J&W) and detected with a flame ionization detector at 300 °C. The injection port was at 170 °C. The gas chromatograph's oven was held at 50 °C for 2 min, then ramped with 15 °C·min^{-1} to 170 °C and eventually 30 °C/min to 240 °C. Column pressure for hydrogen as a carrier gas was 7 psi. Split ratio was 1:40. Peak areas obtained from duplicate vials were averaged and used in the data analysis.

Phase Ratio Variation Headspace Method. A solution of alkanols in water was prepared the same way as described above in the IGS method. Volumes of (0.1, 0.3, 0.5, 1, and 2) mL of this solution were pipetted into five headspace vials with a total volume of 22.3 mL yielding phase ratios in the vials of 222.00,

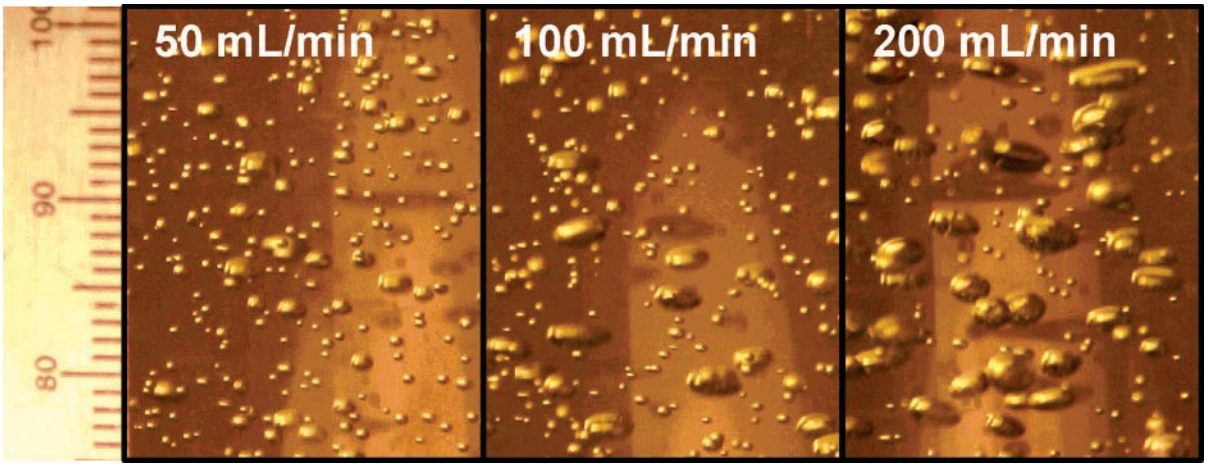

Figure 1. Photographs of the bubbles in the gas-stripping column at different flow rates. The average bubble size increases with increasing gas flow rate.

Table 1. Solute Descriptors for Normal Alkanols,[34] Predictions of Air−Water Partition Coefficient at 25 °C,[29] Adsorption Coefficient on Water Surface at 15 °C,[30] and Enthalpy of Adsorption on the Water Surface[31]

	V	B	A	E	S	L_{16}	log K^{C}_{AW} at 25 °C	log(K_{IA}/m) at 15 °C	$\Delta_{ads}H$/(kJ·mol^{-1})
butan-1-ol	0.73	0.48	0.37	0.224	0.42	2.6	−3.34	−3.03	−68.4
pentan-1-ol	0.87	0.48	0.37	0.219	0.42	3.11	−3.21	−2.71	−72.5
hexan-1-ol	1.01	0.48	0.37	0.21	0.42	3.61	−3.09	−2.39	−76.6
heptan-1-ol	1.15	0.48	0.37	0.211	0.42	4.12	−2.97	−2.07	−80.7
octan-1-ol	1.3	0.48	0.37	0.199	0.42	4.62	−2.85	−1.75	−84.7
nonan-1-ol	1.44	0.48	0.37	0.193	0.42	5.12	−2.72	−1.43	−88.8
decan-1-ol	1.58	0.48	0.37	0.191	0.42	5.63	−2.60	−1.11	−92.9

73.33, 43.60, 21.30, and 10.15, respectively. The alkanol solutions were equilibrated for 60 min at (50, 60, 70, 80 and 90) °C. The time periods required to ensure equilibration had been established in optimization experiments.[28] Peak areas were quantified using the same headspace sampler-gas chromatograph described above. Three sets of vials were prepared and analyzed for each alkanol at each temperature. The reciprocal of the averages of the peak areas obtained from three replicate measurements were regressed against the phase ratio, and a standard deviation for the partition coefficient was estimated by error propagation from the standard error of the linear regression.

Data Analysis. The measured partition coefficients between air and water are being presented in three different but commonly employed units.[28] The water−air partition coefficients K^{C}_{WA} (= $1/K^{C}_{AW}$) (dimensionless, molar concentrations in water and air) derived from slope and intercept of eq 7 are converted to K^{P}_{AW} (in Pa·m^3·mol^{-1}) using

$$K^{P}_{AW} = RT/K^{C}_{WA} \tag{9}$$

where R is the ideal gas constant (8.314 Pa·m^3·mol^{-1}·K^{-1}) and T is absolute temperature (in K). The dimensionless Henry's law constant K^{X}_{AW}, expressed on a mole fraction scale in air and water, can be derived from K^{C}_{WA} by multiplication with the ratio of the molar volumes v_A and v_W of the gas and aqueous phase (m^3·mol^{-1}), respectively:

$$K^{X}_{AW} = 1/K^{C}_{WA}\cdot v_A/v_W \tag{10}$$

The temperature dependence of K^{X}_{AW} is described by the van't Hoff equation:

$$\mathrm{d}\ln K^{X}_{AW}/\mathrm{d}(1/T) = -\Delta_{AW}H/R \tag{11}$$

where $\Delta_{AW}H$ is the enthalpy of the air−water phase transition (J·mol^{-1}). If $\Delta_{AW}H$ is independent of temperature over the range investigated, integration of eq 11 yields

$$\ln K^{X}_{AW} = -\Delta_{AW}H/(RT) + c \tag{12}$$

where c is the constant of integration. Because K^{X}_{AW} is related to the standard Gibbs energy of the air−water phase transition $\Delta_{AW}G^{X}$ (J·mol^{-1}) through

$$\Delta_{AW}G^{X} = -RT\ln K^{X}_{AW} \tag{13}$$

and

$$\Delta_{AW}G^{X} = \Delta_{AW}H - T\Delta_{AW}S^{X} \tag{14}$$

where $\Delta S_{AW}{}^{X}$ is the entropy of the air−water phase transition (J·K^{-1}·mol^{-1}), c equals $\Delta_{AW}S^{X}/R$, and the following relationship can be derived:

$$\ln K^{X}_{AW} = -\Delta_{AW}H/(RT) + \Delta_{AW}S^{X}/R \tag{15}$$

Using eq 15, $\Delta_{AW}H$ and $\Delta_{AW}S^{X}$ were calculated from the slopes and intercepts of the linear regressions between ln K^{X}_{AW} and reciprocal temperature. $\Delta_{AW}G^{X}$ at 25 °C was then calculated using eq 14. Identical values for $\Delta_{AW}G^{X}$ are obtained by inserting the value of K^{X}_{AW} extrapolated to 25 °C into eq 13. $\Delta_{AW}G^{X}$ is the standard free energy computed on the basis of the equilibrium mole fraction in both phases, which is indicated by the superscript X. It is noteworthy that the free energy of transfer is often based on other standard states, such as the unit molar concentration scale. The values of the free energy and entropy of phase transition would then adopt different numerical values.

Model-Based Prediction of K^{C}_{AW} and $K^{C_{app}}_{AW}$. To aid in the data interpretation, K^{C}_{AW} values for the normal alkanols as a function of temperature were estimated using a set of linear

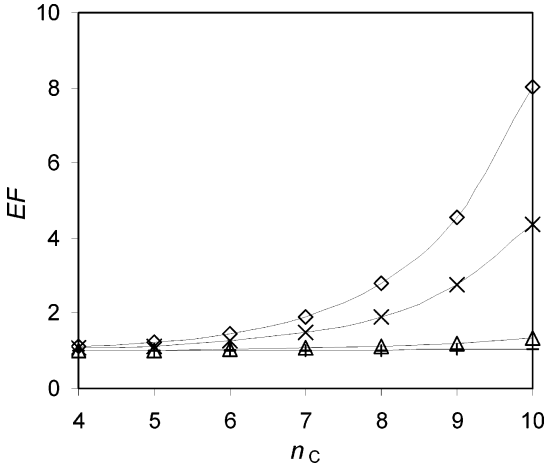

Figure 2. Factor EF by which the apparent air−water partition coefficients of normal alkanols of different chain length n_C is estimated to be enhanced over the real value in inert gas-stripping experiments because of adsorption to the bubble surface: ◇, 25 °C; ×, 31 °C; △, 51 °C; +, 69 °C. A f_{TGB}/r of 1000 m^{-1} was assumed to apply. The EF increases with increasing chain length and decreases with increasing temperature.

solvation energy relationships recently presented by Goss.[29] We further used a polyparameter linear free energy relationship by Roth et al.[30] to estimate the adsorption of the alkanols to the water surface:

$$\log(K_{IA}/m) \text{ at } 15\ ^\circ\text{C} = 0.635 \cdot \log L_{16} + 5.11 \cdot B + 3.60 \cdot A - 8.47 \quad (16)$$

where L_{16} is the heaxadecane/air partition coefficient, and A and B are measures of a solute's hydrogen bonding acidity and basicity. K_{IA} was then adjusted to the experimental temperatures using an enthalpy of adsorption estimated according to Roth et al.:[31]

$$\Delta_{ads}H/(\text{J}\cdot\text{mol}^{-1}) = (-5.52 \ln(K_{IA}/m) - 107) \cdot 1000 \quad (17)$$

There exists a number of other prediction methods for adsorption to the water surface,[32] but the polyparameter linear free energy relationship by Roth et al.[30] was found superior to most of them.[33] The solute descriptors and the predictions of log K^C_{AW} at 25 °C, log(K_{IA}/m) at 15 °C, and $\Delta_{ads}H$ for the alkanols (C4 to C10) are listed in Table 1.

Finally, using predictions of K^C_{AW} and K_{IA} at the experimental temperatures, (eq 5), and the measured bubble radii, the apparent $K_{AW}{}^{C\,app}$ and EF expected from bubble stripping experiments were estimated for a range of f_{TBG} values. Figure 2 displays theoretically estimated EF as a function of temperature and carbon chain length assuming a ratio f_{TGB}/r of 1000 m^{-1}, which would correspond, for example, to a bubble radius of 1 mm and a transfer factor f_{TGB} of 1. Because f_{TGB} cannot be larger than 1 and the average bubble radius in most experiments was slightly larger than 1 mm, these theoretical estimates constitute a maximum EF, unless the prediction method by Roth et al.[30,31] underestimates the K_{IA} values of the alkanols.

Results

Air−Water Partitioning Measured with the Variable Phase Ratio Headspace Technique. Examples of the relationships between reciprocal peak area 1/A and phase ratio β (eq 7) obtained with the PRV−HS technique are shown for heptan-1-ol at various temperatures in Figure 3. These plots show

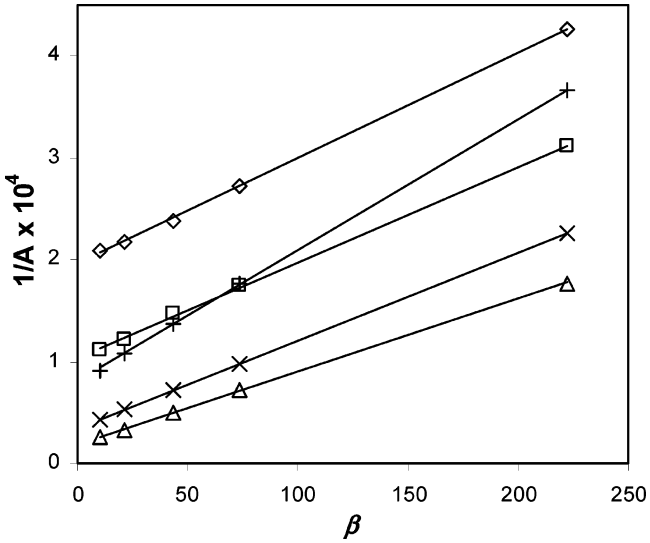

Figure 3. Example of plots of reciprocal peak area vs phase ratio β for heptan-1-ol in an aqueous solution at ◇, 50 °C; □, 60 °C; +, 70 °C; ×, 80 °C; and △, 90 °C. The water−air partitioning coefficient is calculated as the ratio of the intercept and slope of the regressed linear relationships (shown as solid lines).

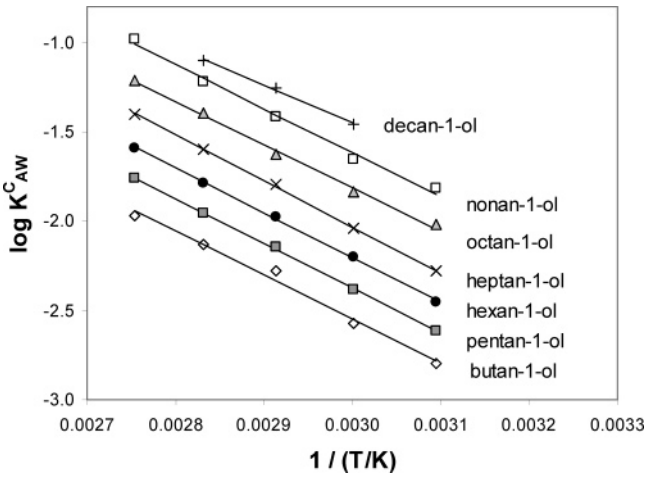

Figure 4. Temperature dependence of the air−water partition coefficient K^C_{AW}, expressed on a molar concentration scale, for seven normal alkanols measured by PRV−HS technique between (50 and 90) °C. The lines are linear regressions of the measured data points.

excellent linearity, with most coefficients of correlation r^2 being 0.999 or higher (Table 2).

The performance of the PRV−HS method depends on achieving large differences in peak area between the different headspace vials, which in turn depends on a wide range of phase ratios.[27,35] With the range of phase ratios employed here (10 to 222), the highest liquid−gas partition coefficient that can be determined reliably is around 1000. For such a substance the difference between the peak areas obtained from the vials with the smallest and largest phase ratio is about 20 %. It is for this reason that the relationships between 1/A and β are less linear for the larger K^C_{WA} values (i.e., for the shorter alkanols at lower temperatures). This is also the reason why the PRV−HS method is unsuitable for measuring the K^C_{WA} of the short-chain alkanols at temperatures lower than 50 °C and why the data for butan-1-ol reported here are somewhat less reliable than those for the longer alkanols. In general, the individual measured partition coefficients have a coefficient of variation (CV) of 5 % or less (Table 2). Only the partition coefficients measured at 90 °C have a considerably higher CV of more than 10 %, presumably

Table 2. Slopes, Intercepts, and Correlation Coefficient (r^2) of the Linear Regression of Reciprocal Peak Area 1/*A* vs Phase Ratio β and Air−Water Partition Coefficients for Seven Normal Alkanols Derived from These Regressions

compound	*T*/°C	slope	intercept	r^2	K^{C}_{AW}	K^{P}_{AW}/Pa·m^3·mol^{-1}	K^{X}_{AW}
butan-1-ol	50	$8.47\cdot10^{-7}$	$5.32\cdot10^{-4}$	0.986	630 ± 19	4.3 ± 0.1	2.3 ± 0.1
	60	$8.33\cdot10^{-7}$	$3.11\cdot10^{-4}$	0.996	373 ± 9	7.4 ± 0.2	4.1 ± 0.1
	70	$1.62\cdot10^{-6}$	$3.06\cdot10^{-4}$	0.997	190 ± 9	15.0 ± 0.7	8.2 ± 0.4
	80	$9.18\cdot10^{-7}$	$1.24\cdot10^{-4}$	0.999	135 ± 2	21.8 ± 0.2	11.9 ± 0.1
	90	$7.36\cdot10^{-7}$	$6.84\cdot10^{-5}$	0.998	93 ± 9	32.6 ± 3.3	17.7 ± 1.8
pentan-1-ol	50	$1.08\cdot10^{-6}$	$4.42\cdot10^{-4}$	0.988	410 ± 9	6.5 ± 0.1	3.6 ± 0.1
	60	$9.98\cdot10^{-7}$	$2.43\cdot10^{-4}$	0.994	244 ± 10	11.4 ± 0.5	6.2 ± 0.3
	70	$1.46\cdot10^{-6}$	$2.05\cdot10^{-4}$	0.999	140 ± 5	20.4 ± 0.7	11.2 ± 0.4
	80	$9.43\cdot10^{-7}$	$8.58\cdot10^{-5}$	0.999	91 ± 4	32.3 ± 1.6	17.7 ± 0.9
	90	$7.76\cdot10^{-7}$	$4.48\cdot10^{-5}$	1.000	58 ± 2	52.3 ± 2.1	28.6 ± 1.2
hexan-1-ol	50	$1.08\cdot10^{-6}$	$3.06\cdot10^{-4}$	0.997	283 ± 15	9.5 ± 0.5	5.2 ± 0.3
	60	$1.03\cdot10^{-6}$	$1.65\cdot10^{-4}$	0.998	159 ± 4	17.4 ± 0.5	9.5 ± 0.3
	70	$1.47\cdot10^{-6}$	$1.39\cdot10^{-4}$	1.000	94 ± 4	30.4 ± 1.3	16.6 ± 0.7
	80	$9.33\cdot10^{-7}$	$5.70\cdot10^{-5}$	1.000	61 ± 3	48.1 ± 2.1	26.3 ± 1.1
	90	$7.84\cdot10^{-7}$	$3.06\cdot10^{-5}$	0.999	39 ± 5	78 ± 10	45 ± 5
heptan-1-ol	50	$1.03\cdot10^{-6}$	$1.96\cdot10^{-4}$	0.999	190 ± 4	14.2 ± 0.3	7.8 ± 0.2
	60	$9.38\cdot10^{-7}$	$1.04\cdot10^{-4}$	0.999	110 ± 2	25.1 ± 0.5	13.7 ± 0.3
	70	$1.34\cdot10^{-6}$	$8.43\cdot10^{-4}$	1.000	63 ± 2	45.5 ± 1.7	24.9 ± 0.9
	80	$8.62\cdot10^{-7}$	$3.41\cdot10^{-5}$	1.000	39.5 ± 1.3	74.3 ± 2.6	40.7 ± 1.4
	90	$7.18\cdot10^{-7}$	$1.80\cdot10^{-5}$	1.000	25 ± 4	122 ± 17	66 ± 9
octan-1-ol	50	$1.42\cdot10^{-6}$	$1.50\cdot10^{-4}$	0.999	105 ± 6	25.6 ± 1.4	14.0 ± 0.8
	60	$1.12\cdot10^{-6}$	$7.76\cdot10^{-5}$	0.999	69 ± 4	40.1 ± 2.1	21.9 ± 1.2
	70	$1.47\cdot10^{-6}$	$6.31\cdot10^{-5}$	1.000	42.6 ± 2.3	67.2 ± 3.6	36.7 ± 2.0
	80	$9.63\cdot10^{-7}$	$2.38\cdot10^{-5}$	1.000	24.7 ± 0.5	119 ± 3	65.1 ± 1.4
	90	$7.81\cdot10^{-7}$	$1.27\cdot10^{-5}$	1.000	16.3 ± 2.5	189 ± 31	102 ± 15
nonan-1-ol	50	$1.76\cdot10^{-6}$	$1.15\cdot10^{-4}$	0.997	65.5 ± 3.6	41.1 ± 2.3	22.5 ± 1.2
	60	$1.28\cdot10^{-6}$	$5.82\cdot10^{-5}$	0.998	45.5 ± 2.4	61.0 ± 3.2	33.4 ± 1.8
	70	$1.61\cdot10^{-6}$	$4.23\cdot10^{-5}$	1.000	26.1 ±1.4	109 ± 6	59.9 ± 3.1
	80	$9.67\cdot10^{-7}$	$1.61\cdot10^{-5}$	1.000	16.7 ± 0.6	176 ± 6	96.5 ± 3.3
	90	$7.94\cdot10^{-7}$	$7.48\cdot10^{-6}$	0.999	9.6 ± 3.4	350 ± 144	173 ± 62
decan-1-ol	60	$1.68\cdot10^{-6}$	$4.85\cdot10^{-5}$	0.997	28.9 ± 0.4	95.9 ± 1.4	52.5 ± 0.8
	70	$1.77\cdot10^{-6}$	$3.23\cdot10^{-5}$	1.000	18.1 ± 1.6	159 ± 14	87 ± 7
	80	$9.74\cdot10^{-7}$	$1.23\cdot10^{-5}$	1.000	12.6 ± 0.7	234 ± 13	128 ± 7

Table 3. Regression Parameters (Slope, Intercept, Coefficient of Correlation) of the Linear Regression between the Logarithm of Air−Water Partition Coefficients (log K^{C}_{AW}) and Reciprocal Absolute Temperature, Air−Water Partition Coefficients Extrapolated to 25 °C, and Thermodynamic Parameters for Air−Water Phase Transition for Seven Normal Alkanols

compounds	butan-1-ol	pentan-1-ol	hexan-1-ol	heptan-1-ol	octan-1-ol	nonan-1-ol	decan-1-ol
slope for log K^{C}_{AW} vs 1/*T*	−(2472 ± 151)	−(2501 ± 39)	−(2509 ± 46)	−(2585 ± 33)	−(2425 ± 87)	−(2467 ± 133)	−(2122 ± 126)
intercept for log K^{C}_{AW} vs 1/*T*	4.9 ± 0.4	5.1 ± 0.1	5.3 ± 0.1	5.7 ± 0.1	5.5 ± 0.2	5.8 ± 0.4	−4.9 ± 0.4
r^2 for log K^{C}_{AW} vs 1/*T*	0.989	0.999	0.999	1.000	0.996	0.991	0.996
log K^{C}_{AW} at 25 °C	−(3.43 ± 0.67)	−(3.26 ± 0.17)	−(3.09 ± 0.20)	−(2.95 ± 0.15)	−(2.67 ± 0.39)	−(2.49 ± 0.59)	−(2.20 ± 0.56)
log(K^{P}_{AW}/Pa·m^3·mol^{-1}) at 25 °C	−(0.03 ± 0.67)	0.12 ± 0.17	0.30 ± 0.20	0.45 ± 0.15	0.72 ± 0.39	0.90 ± 0.59	1.19 ± 0.56
log K^{X}_{AW} at 25 °C	−(0.29 ± 0.67)	−(0.13 ± 0.17)	0.04 ± 0.20	0.19 ± 0.15	0.46 ± 0.39	0.64 ± 0.59	0.93 ± 0.56
$\Delta_{AW}H$/kJ·mol^{-1}	50.2 ± 2.9	50.7 ± 0.7	50.9 ± 0.8	52.3 ± 0.6	49.3 ± 1.7	50.1 ± 2.6	43.5 ± 2.4
$T\Delta_{AW}S^{X}$/kJ·mol^{-1}	48.5 ± 2.5	50.0 ± 0.6	51.1 ± 0.7	53.4 ± 0.5	51.9 ± 1.5	53.7 ± 2.2	48.8 ± 2.1
$\Delta_{AW}G^{X}$/kJ·mol^{-1} at 25 °C	−(1.7 ± 3.8)	0.8 ± 1.0	−(0.2 ± 1.1)	−(1.0 ± 0.8)	−(2.6 ± 2.2)	−(3.6 ± 3.4)	−(5.3 ± 3.2)
$\Delta_{AW}S^{X}$/J·K^{-1}·mol^{-1}	163 ± 8	168 ± 2	171 ± 2	179 ± 2	174 ± 5	180 ± 8	164 ± 7

because, at temperatures so close to the boiling point, water is condensing at the top of the headspace vials interfering with the partitioning process. For decan-1-ol, this prevented the determination of reliable partition coefficients at 90 °C.

All experimentally determined air−water partition coefficients are listed in Table 2 and are displayed as a function of reciprocal absolute temperature in Figure 4. Clearly, the air−water partition coefficient is increasing with increasing chain length and increasing temperature. The fact that the regression lines in Figure 4 are parallel indicates that the temperature dependence of the K^{C}_{AW} of different alkanols is similar, yielding an enthalpy of water-gas transition of approximately 50 kJ·mol^{-1} (Table 3). The fact that the lines are more or less equidistant from each other suggests that the increase in K^{C}_{AW} with each additional -CH_2- unit is uniform, namely, 0.21 ± 0.03 log units per methylene. The relationships between log K^{C}_{AW} and 1/*T* are highly linear within the investigated temperature range (Table 3), in particular for pentan-1-ol, hexan-1-ol, and heptan-1-ol ($r^2 > 0.999$). For the reason stated above, the linearity of the relationship for butan-1-ol is somewhat lower ($r^2 = 0.989$). Because of the high linearity of the relationships it is possible to estimate the air−water partition coefficient at 25 °C by extrapolation of the experimental values to lower temperatures. These estimates are included in Table 3. The reported uncertainty for these values includes the propagation of the uncertainty of the slope and intercept of the log K^{C}_{AW} versus 1/*T* relationship. This uncertainty is quite substantial for butan-1-ol, nonan-1-ol, and decan-1-ol but surprisingly small for pentan-1-ol, hexan-1-ol, and heptan-1-ol considering the need to extrapolate over a 25 K temperature range.

Comparison with Literature Values. Experimentally determined air−water partition coefficients at the temperatures of the headspace measurements described here have been reported for butan-1-ol by Kolb et al.;[36] for butan-1-ol and pentan-1-ol by Vrbka et al.;[37] and for butan-1-ol, pentan-1-ol, and hexan-1-ol by Gupta et al.[38] Figure 5 compares the new experimental data with these literature values within the temperature range of (40 to 90) °C. Agreement between the measurements reported here with those by Vrbka et al.[37] is excellent, in particular for pentan-1-ol. However, the values reported by Kolb et al.[36] and

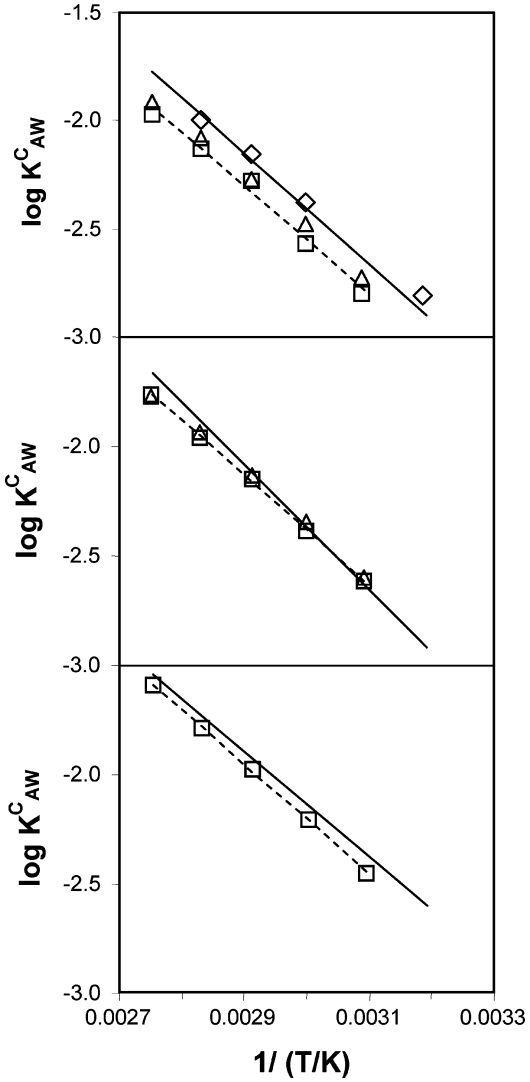

Figure 5. Comparsion of the air−water partition coefficient K_{AW}^{C} for butan-1-ol (top panel), pentan-1-ol (middle panel), and hexan-1-ol (bottom panel) measured in this study (□, broken line indicates regression through measured data), with those reported by ◇, ref 36; —, ref 38; and △, ref 37.

Gupta et al.[38] for butan-1-ol are somewhat higher than those reported here and by Vrbka et al.[37] Agreement of the Gupta et al.[38] values with other studies is better for pentan-1-ol and hexan-1-ol. We consider the data by Vrbka et al.[37] the best reference values and superior to other reported values because these authors could demonstrate small scatter, good agreement between different methods, and thermodynamic consistency. Based on the agreement with the values by Vrbka et al.,[37] we thus judge the values obtained here with the PRV−HS method as reliable.

Experimentally determined air−water partition coefficients at 25 °C for normal alkanols up to a chain length of five, six, and eight carbons have been reported by Vrbka et al.,[37] Gupta et al.,[38] and Butler et al.,[39] respectively. Burnett[40] and Snider and Dawson[41] report such values for methanol, ethanol, propan-1-ol, and butan-1-ol. Buttery et al.[42] reported air−water partitioning data for butan-1-ol, hexan-1-ol, and octan-1-ol. Shiu and Mackay[7] measured the Henry's law constant of heptan-1-ol with the IGS technique. With the exception of the latter value, which appears too high when compared to the other experimental values, these experimental data can be fitted well to an equation relating linearly the log K_{AW}^{C} with the length of the carbon chain (Figure 6). It is also possible to estimate the air−water partition coefficients at 25 °C for normal alkanols from numerous measurements of the vapor pressure and water solubility reported in the handbook of Mackay et al.[43] These estimates are in excellent agreement with the reported literature values (Figure 6).

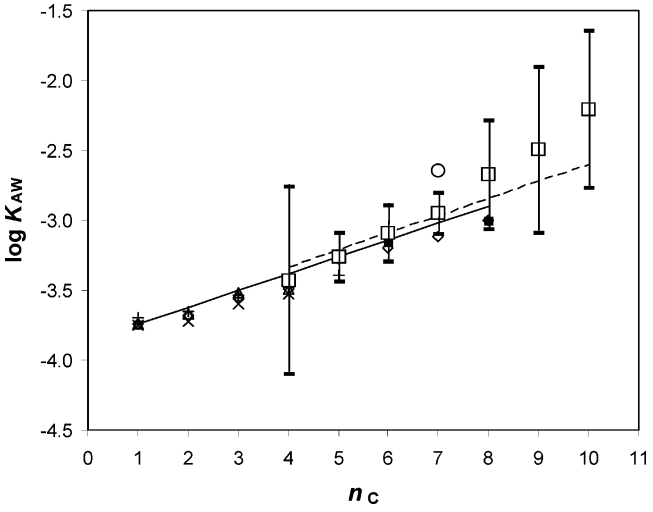

Figure 6. Comparison of the K_{AW}^{C} for alkan-1-ol (C1 to C10, displayed as function of carbon chain length n_C) at 25 °C extrapolated from the headspace measurements at higher temperatures reported here (□ with whiskers indicating uncertainty) with those reported in the literature (◇, ref 39; ×, ref 40; △, ref 41; ■, ref 42; ○, ref 7; +, ref 37) calculated from vapor pressure and water solubility data reported in ref 43 (—) and estimated from linear solvation energy relationships reported by ref 29 (− −).

The K_{AW}^{C} values at 25 °C for butan-1-ol to octan-1-ol, extrapolated from the PRV−HS measurements at higher temperatures reported here, agree very well with the measured values reported in the literature and with the values estimated from vapor pressure and water solubility (Figure 6). No previous measurements of the K_{AW}^{C} of nonan-1-ol or decan-1-ol have been reported, and the extrapolated values reported here have a fairly large uncertainty. Within the experimental error they are in agreement with estimates of K_{AW}^{C} from vapor pressure and water solubility. All experimental values are also in good agreement with K_{AW}^{C} values estimated with the help of the linear solvation energy relationships by Goss.[29]

Results of the Inert Gas-Stripping Experiments. Figure 7 displays the result of the IGS experiments at (69 and 31) °C and a nominal flow rate of 200 mL·min^{-1}. The plots of ln(A/A_0) against t/V(t) at 69 °C were highly linear (Figure 7A). As is obvious from the increase in slope in these plots from butan-1-ol to decan-1-ol, the rate of disappearance from the water column greatly increased with the length of an alkanol's carbon chain. At 69 °C the long-chain alkanols were lost from the stripping column almost immediately: after 0.5 h of stripping, 95 % of the decan-1-ol present at the onset of stripping had already disappeared. It is for this reason that $K_{AW}^{C_{app}}$ for decan-1-ol and nonan-1-ol could only be determined very approximately at higher experimental temperatures. For longer chain alkanols (C7 and longer) at lower temperatures (25, 31, and 51 °C) the plots of ln(A/A_0) against t/V(t) were no longer perfectly linear (Figure 7B) but clearly showed a distinct change in slope during the experiment. The change in slope occurred earlier and was more pronounced with increasing chain length. For example, at 31 °C the change in slope for heptan-1-ol was hardly noticeable, whereas decan-1-ol was lost very slowly after an initial very rapid loss (Figure 7B). The change in slope indicates that at different times during the experiment different processes are rate limiting for the loss of chemical from the

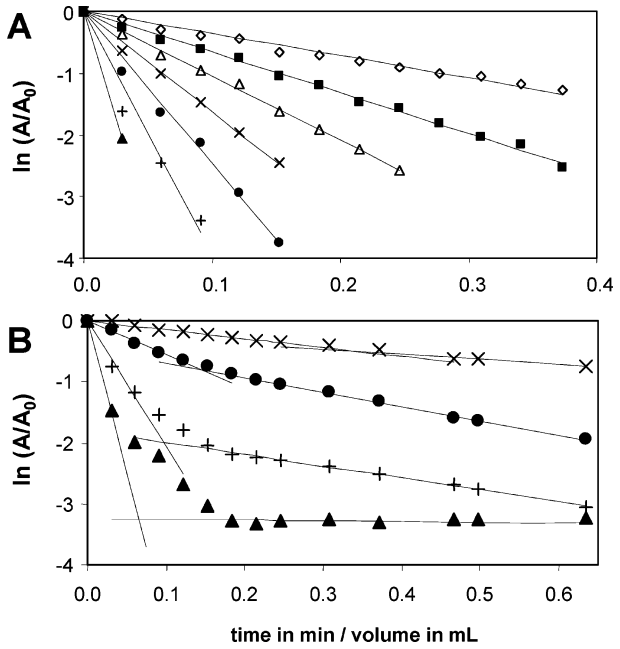

Figure 7. Plot indicating the gradual loss of alkanols (◇, butan-1-ol; ■, pentan-1-ol; △, hexan-1-ol; ×, heptan-1-ol; ●, octan-1-ol; +, nonan-1-ol; ▲, decan-1-ol) from aqueous solution during IGS at a temperature of 69 °C (A) and 31 °C (B) and a nominal flow rate of 200 mL·min^{-1}. The solid lines are linear regressions of all (panel A) or a selection (panel B) of the displayed measured data.

water column. Initially, the sparging of the chemical from the dissolved aqueous phase is rate determining. After a large fraction of the chemical has been lost from the water column, the replenishment of the dissolved phase with chemical adsorbed at the glass walls of the stripping vessel becomes rate-limiting. The rate of desorption from the glass wall should be slower and should become rate-limiting earlier for longer alkanols, because their dissolved fraction is rapidly depleted by the stripping gas. We would also expect this wall sorption effect to be more pronounced at lower temperatures, which may explain why no such change in slope was observed at 69 °C. Only the initial slopes were used in the derivation of $K_{AW}^{C_{app}}$.

Evaporation Effect on Results of IGS Experiments. The apparent partition coefficient between air and water derived from the IGS experiments are listed in Table 4. The values for butan-1-ol at different temperatures obtained by PRV−HS and IGS methods are compared in the left panel, those for all seven normal alkanols at 69 °C are compared in the right panel of Figure 8. In both cases, the IGS method yielded consistently higher values than the PRV−HS method. The example of butan-1-ol shows that the difference between the methods is larger at higher temperatures than at low temperatures (Figure 8). The difference at 69 °C is quite similar for different alkanols (i.e., the IGS methods yielded partition coefficients that are approximately five times larger than those measured by PRV−HS). Because the PRV−HS was judged to yield accurate results by comparison with literature data, this implies that the IGS method consistently overestimates the partition coefficient between air and water. This discrepancy between the methods cannot be explained by sorption to the bubble surface. As displayed in Figure 2, the surface sorption effect is not expected to affect either IGS measurements of a chemical with a relatively small K_{IA} such as butan-1-ol, nor those of alkanols at temperatures as high as 69 °C. Furthermore, a surface sorption effect would not be expected to equally affect the IGS measurements of alkanols of different chain length but would lead to larger artefacts for longer chain alkanols. Finally, the effect of surface sorption would be larger at low than at high temperature.

Table 4. Apparent Water−Air Partition Coefficients Determined by IGS at Different Temperatures *T* and Gas Flow Rates *G*[a]

	T	*G*				$K_{AW}^{P_{app}}$
compound	°C	mL·min^{-1}	*n*	r^2	$K_{WA}^{C_{app}}$	Pa·m^3·mol^{-1}
butan-1-ol	25	100	12	0.999	2003 ± 23	1.24 ± 0.01
	31	200	29	0.997	1249 ± 18	1.98 ± 0.03
	51	200	14	0.989	184 ± 4	13.5 ± 0.3
	51	50	25	0.994	200 ± 3	12.4 ± 0.2
	69	200	13	0.981	55.6 ± 1.2	44.6 ± 1.0
penta-1-ol	25	100	37	0.999	1313 ± 15	1.89 ± 0.02
	31	200	29	0.998	752 ± 10	3.30 ± 0.04
	51	200	14	0.997	106 ± 1	23.4 ± 0.3
	51	50	25	0.996	125 ± 2	19.8 ± 0.2
	69	200	13	0.995	30.3 ± 0.4	81.8 ± 1.1
hexan-1-ol	25	100	11	0.993	489 ± 14	5.1 ± 0.1
	25	200	10	0.952	466 ± 35	5.3 ± 0.4
	31	200	25	0.998	482 ± 7	5.1 ± 0.1
	51	200	14	0.997	68.5 ± 0.9	36.2 ± 0.5
	51	50	25	0.998	80.2 ± 0.9	30.9 ± 0.3
	69	200	9	0.997	19.1 ± 0.3	130 ± 2
heptan-1-ol	25	100	10	0.989	190 ± 4	13.1 ± 0.3
	25	200	11	0.984	201 ± 8	12.3 ± 0.5
	31	200	9	0.994	138 ± 4	17.9 ± 0.5
	51	200	14	0.997	47.2 ± 0.6	52.5 ± 0.7
	51	50	14	0.991	47.2 ± 0.8	52.5 ± 0.9
	69	200	6	0.994	12.3 ± 0.2	202 ± 4
octan-1-ol	25	100	11	0.999	71 ± 1	35.1 ± 0.5
	25	200	11	0.998	72 ± 1	34.4 ± 0.6
	31	200	5	0.996	36 ± 1	69 ± 2
	51	200	6	0.997	23.8 ± 0.4	104 ± 2
	51	50	5	0.955	17.6 ± 1.0	141 ± 8
	69	200	6	0.997	8.1 ± 0.2	306 ± 8
nonan-1-ol	25	100	3	0.981	9.4 ± 0.9	265 ± 26
	25	200	9	0.998	36 ± 0.7	68.7 ± 1.3
	31	200	3	0.988	9.7 ± 0.8	255 ± 20
	51	200	4	0.997	10.4 ± 0.2	238 ± 5
	51	50	3	0.964	6.2 ± 0.5	400 ± 33
	69	200	4	0.988	5.1 ± 0.3	488 ± 31
decan-1-ol	25	100	2	n.a.	(3.1)	(791)
	25	200	7	0.992	22 ± 1	114 ± 4
	31	200	2	n.a.	(4.1)	(608)
	51	200	2	n.a.	(2.9)	(848)
	51	50	2	n.a.	(2.2)	(1109)
	69	200	2	n.a.	(2.9)	(848)

[a] Also given are the number of data points *n* and the coefficient of correlation r^2 of the $\ln(A/A_0)$ vs $V(t)/t$ regressions.

We believe that at relatively high experimental temperatures, evaporation of chemical from the stripping column becomes significant. There are several indications for this to be the case: First, as described in the Experimental Section, the alkanol solution was allowed to sit in the stripping apparatus at the experimental temperature for one night prior to the start of the gas flow. At higher temperatures, significant fractions of the alkanols were lost from the apparatus during this period even in the absence of a gas flow (left panel of Figure 9). We infer that air enters the stripping vessel to replace air that is convected out of the vessel, especially at high temperatures. The loss increased with increasing length of the alkanol and with increasing temperature (i.e., is related to the alkanol's K_{AW}^{C}). For example, as much as 80 % of the decan-1-ol had been lost from the solution before the onset of gas-stripping at 69 °C. At (51 and 69) °C even the concentrations of the shorter chain alkanols decreased appreciably overnight.

Second, an experiment resembling the IGS experiment at 69 °C was performed but without any gas being supplied to the stripping vessel. The concentrations in the aqueous phase displayed a similar decrease as was observed in IGS experiments (right panel of Figure 9), although at a considerably lower rate.

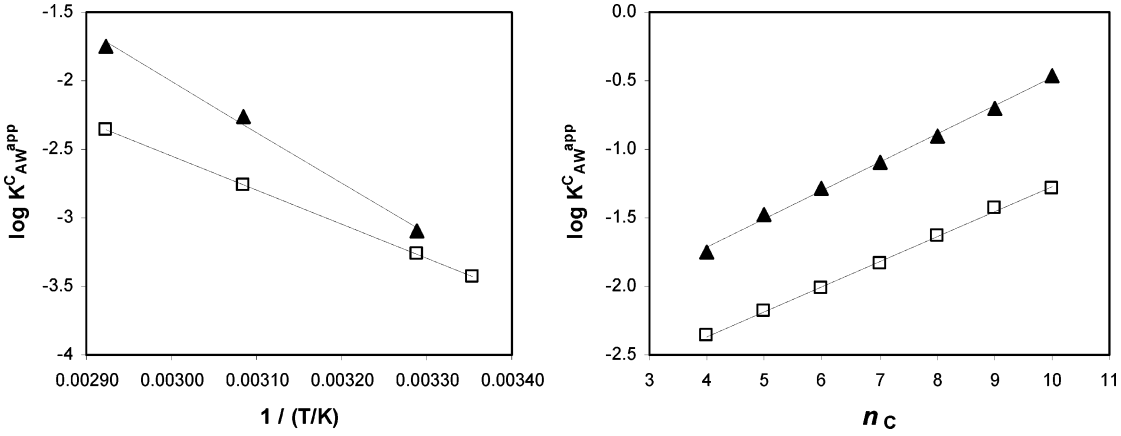

Figure 8. Comparison of the air−water partition coefficients for butan-1-ol at different temperatures (left panel) and for seven alkanols (C4 to C10, displayed as function of carbon chain length n_C) at 69 °C (right panel) measured with the phase ratio variation headspace (□) and inert gas-stripping methods (▲). The lines indicate linear regressions of the measured data.

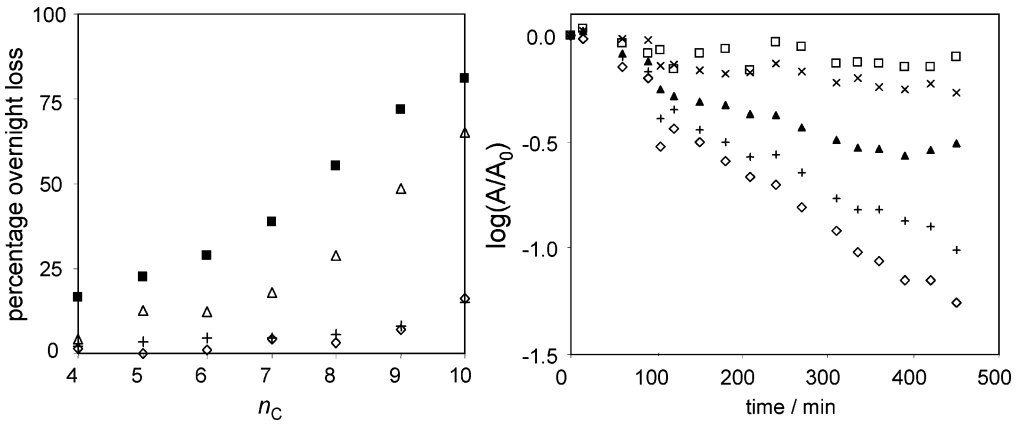

Figure 9. Experimental results indicating the loss of alkanols from the gas-stripping vessel in the absence of a stripping gas. The left panel displays the percentage loss of alkanols from the vessel in the night prior to the stripping experiments at different temperatures (+, 25 °C; ◇, 31 °C; △, 51 °C; ■, 69 °C; displayed as function of carbon chain length n_C), and the right panel displays the decline in water concentration of several alkanols (□, pentan-1-ol; ×, heptan-1-ol; ▲, octan-1-ol; +, nonan-1-ol; ◇, decan-1-ol) during an experiment at 69 °C without gas flow.

Water that had condensed at the top of the glass stripping vessel was analyzed for the alkanols and had concentrations in excess of the initial water concentrations—in the case of the longer chain alkanols often higher by more than an order of magnitude. Essentially, at higher experimental temperatures the stripping vessel functions like a distillation column, distilling the alkanols out of the water solution. We suspect that the relatively poor linearity of the $\ln(A/A_0)$ versus time plots of the experiment without gas flow (Figure 9) was caused by drops of condensed water, highly enriched in alkanols, falling back into the stripping vessel and causing a sudden increase in water concentrations.

Evaporation of chemical from the stripping vessel may explain the unreasonably high values obtained by IGS displayed in Figure 8. Evaporation losses increase with temperature (left side of Figure 8) and are proportional to K^{C}_{AW} and thus lead to a similar relative error in the measured $K^{C_{app}}_{AW}$ for different chemicals (right side of Figure 8). We cannot use the slopes from the right panel of Figure 9 to quantify the evaporation error during the IGS experiment at the same temperature. Evaporation loss may be higher during an experiment with gas flow than in the experiment displayed in Figure 9, because the stripping gas will increase the turbulence in both water and gas phase and therefore speed up evaporation.

Effect of Adsorption to the Bubble Surface on Results of IGS Experiments. In order to assess the occurrence and extent of a surface adsorption effect on the result of the IGS experiment, it is necessary to account for the evaporation effect discussed in the previous section. To do this we make two assumptions. The first is that the evaporation effect leads to a similar relative error for all alkanols (i.e., it causes the $K^{C_{app}}_{AW}$ to be higher than the K^{C}_{AW} by a constant factor; right side of Figure 8). The second is to assume that for butan-1-ol, adsorption to the water surface is not important at any of the experimental temperatures (Figure 2). We can then use the factor by which the $K^{C_{app}}_{AW}$ for butan-1-ol from the IGS experiments is higher than the K^{C}_{AW} for butan-1-ol from the PRV−HS experiments to calculate the enhancement factor for an alkanol that is NOT due to the evaporation effect:

$$EF_{measured}(alk.) = [K^{C_{app}}_{AW}(alk.)/K^{C}_{AW}(alk.)]\cdot[K^{C}_{AW}(but.)/K^{C_{app}}_{AW}(but.)] \quad (18)$$

If we call the ratio between the results of the IGS and PRV−HS experiments the total enhancement factor EF_{total}, which includes the effect of both evaporation and surface adsorption, eq 18 can be rewritten as follows:

$$EF_{measured}(alk.) = EF_{total}(alk.)/EF_{total}(but.) \quad (19)$$

Of course, $EF_{measured}$ for butan-1-ol is by definition equal to 1. Care must be taken that the EF_{total} for alkanol and butan-1-ol in eq 19 apply to the same experimental conditions (i.e., temperature and gas flow rate). Because no $K^{C_{app}}_{AW}$ for butan-1-ol could be determined in the IGS experiment at 25 °C and

Table 5. Enhancement Factors Expressing the Extent to Which $K_{AW}^{C_{app}}$ Values for Normal Alkanols Determined with the IGS Technique Exceed the K_{AW}^{C} Value Determined by the PRV−HS Method[a]

T/°C	G/mL·min^{-1}	butan-1-ol	pentan-1-ol	hexan-1-ol	heptan-1-ol	octan-1-ol	nonan-1-ol	decan-1-ol
				EF_{total}				
25	200	na	na	2.7	4.4	6.5	8.6	7.3
25	100	1.3	1.4	2.5	4.7	6.7	33	51
31	200	1.5	1.7	1.8	4.3	9.0	22	28
51	200	3.1	3.7	3.8	3.8	4.4	6.5	15
51	50	2.9	3.1	3.3	3.8	6.0	11	19
69	200	4.1	5.0	5.4	5.5	5.2	5.3	6.6
				$EF_{measured}$				
25	200	na	na	2.0	3.3	4.9	6.5	6
25	100	1.0	1.0	1.9	3.5	5.0	25	38
31	200	1.0	1.1	1.2	3.0	6.2	15	19
51	200	1.0	1.2	1.2	1.2	1.4	2.1	4.7
51	50	1.0	1.1	1.1	1.3	2.1	3.8	6.6
69	200	1.0	1.2	1.3	1.3	1.3	1.3	1.6

[a] EF_{total} and $EF_{measured}$ express the total enhancement and the enhancement caused by surface adsorption only, respectively.

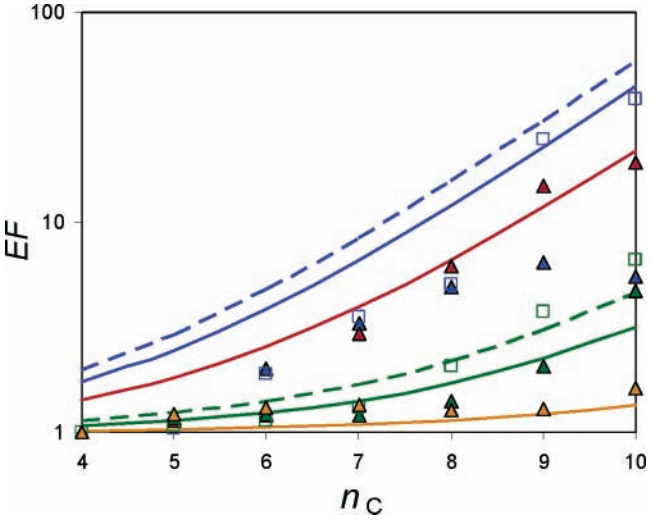

Figure 10. Comparison of theoretically estimated (lines) and measured (markers) enhancement factors EF for normal alkanols (displayed as function of carbon chain length n_C) at different experimental temperatures (blue for 25 °C, red for 31 °C, green for 51 °C, yellow for 69 °C) and gas flow rates (filled triangles and solid lines for 200 mL·min^{-1}, open squares and broken lines for 50 and 100 mL·min^{-1}). The enhancement factors express the extent to which air−water partition coefficients are elevated as a result of adsorption to the bubble surface.

200 mL·min^{-1}, the $K_{AW}^{C_{app}}$ for butan-1-ol from the experiment with 100 mL·min^{-1} was used instead.

Table 5 lists the EF_{total} and $EF_{measured}$ for the seven normal alkanol from all six IGS experiments. We can make the following observations: (i) $EF_{measured}$ increases with increasing chain length of the alkanol; (ii) $EF_{measured}$ increases with decreasing experimental temperature; and (iii) $EF_{measured}$ is generally higher at lower flow rates, which lead to smaller bubbles and higher surface-to-volume ratios. All three observations are consistent with what would be expected from an artifact caused by adsorption to the bubble surface[21] (Figure 2). Figure 10 compares the $EF_{measured}$ with theoretically derived EF as defined in eq 5. In the estimation of EF the K_{IA} values predicted with the help of eqs 16 and 17, a f_{TGB} of 1, and the bubble radii r derived from the digital photographs (Figure 1) were employed.

The comparison of theoretical (lines) and measured (markers) enhancement factors in Figure 10 shows that they not only follow the same trends with temperature, chain length and flow rate (i.e., bubble size) but are also of the same order of magnitude. Such agreement must be judged very good, considering the uncertainty in the prediction of K_{IA} values at different temperatures, the uncertainty in f_{TGB}, the potential error introduced in the butan-1-ol normalization of eq 18, and the experimental error in K_{AW}^{C} and $K_{AW}^{C_{app}}$. The results thus clearly demonstrate that adsorption to the water surface can significantly affect the result of IGS experiments,[21] especially at low temperatures and for substances with a large K_{IA}. Under the conditions of the IGS experiment conducted here, K_{IA} values on the order of 1 mm led to significant errors in the measured air−water partitioning. This makes intuitive sense, as we would expect the surface adsorption process to matter if the K_{IA} and the dimensions of the bubbles are of the same order of magnitude.

Discussion

The present investigation has identified three processes that can cause the widely used IGS technique for the determination of air−water partition coefficients to yield erroneous results. The three processes only affect some chemicals under some experimental conditions.

Rapid Depletion of Dissolved Phase and Sorption to the Vessel Walls. The experiments with longer chain alkanols at lower temperatures revealed that the graphs plotting the decrease in water concentrations as the experiment progresses can display distinct changes in slope (Figure 7B). We attributed this change in slope to a change in the rate-limiting step from the stripping of dissolved phase chemical from the water column to the desorption of chemical adsorbed to the vessel wall into the water column. This phenomenon could result in erroneous interpretation of IGS results in two ways. In cases where the slope change is subtle (e.g., heptan-1-ol in Figure 7B) and the number of data points is small, a linear regression may be drawn through sections of the graph representing different phases of the experiment. In cases where the slope change occurs early on in the experiment (e.g., nonan-1-ol or decan-1-ol in Figure 7B) and sampling only starts after a preliminary period of stripping, the first and only relevant phase of the experiment may be missed entirely. In both cases, the erroneous interpretation would lead to K_{AW}^{C} values that are lower than the real values because the slope of the $\ln(A/A_0)$ versus time/volume relationship (eq 3) would be underestimated. This effect is most relevant for substances that adsorb strongly to the glass surface of the stripping vessel and that are rapidly purged from the water column (i.e., those with high K_{AW}^{C} values). It is also more pronounced at lower experimental temperatures, which implies that it would overestimate the temperature dependence of K_{AW}^{C} (i.e., yield erroneously large $\Delta_{AW}H$ values).

Evaporation from the Stripping Vessel at High Temperatures. The IGS experiments described here show that normal alkanols are stripped from the stripping vessel faster than expected based on their K_{AW}^{C} values because of evaporation from the stripping vessel. The occurrence of such evaporation is obvious from the loss of chemicals from the water column even in the absence of a stripping gas flow. This evaporation effect appears to affect all chemicals to the same extent (i.e., $K_{AW}^{C_{app}}$ values are too high by a similar factor). It is strongest at higher temperatures, ranging from a factor of approximately 1.3 at 25 °C to a factor of 4 at 69 °C (Table 5). This effect leads to an overestimation of K_{AW}^{C}, particularly at high temperatures. It thus leads to erroneously large $\Delta_{AW}H$ values. For example, the log $K_{AW}^{C_{app}}$ versus $1/T$ relationship displayed in the left panel of Figure 8 would have yielded a $\Delta_{AW}H$ of 72 kJ·mol^{-1} for butan-1-ol, much higher than the 50 kJ·mol^{-1} derived from the PRV−HS measurements.

Adsorption to the Bubble Surface. The experiments described here provide evidence that adsorption of chemical to the bubble surface can lead to $K_{AW}^{C_{app}}$ values in IGS experiments that are too high. It is particularly relevant if the bubbles generated in the IGS column are small, because that leads to a high surface area-to-volume ratio. This effect is only important for substances that adsorb strongly to the water surface ($\log(K_{IA}/m) > -2$) and, because interfacial sorption increases with decreasing temperatures, is most pronounced at low temperatures. In contrast to the other two processes described above, it thus leads to an underestimation of the temperature dependence of air−water partitioning and $\Delta_{AW}H$ values that are too low. For highly sorptive chemicals, such as decan-1-ol investigated here, the effect can be so strong that no apparent temperature dependence is obvious in the $K_{AW}^{C_{app}}$ values measured by IGS (Table 4).

The artefacts caused by evaporation and adsorption to the bubble surface would equally affect the so-called modified IGS method,[12,13] which relies on the quantification of the concentrations in the stripped gas in addition to the water column and derives the K_{AW}^{C} from the ratio of the two concentrations. Please note that the surface adsorption artifact does not require the formation of an aerosol upon bubble bursting[13,22] but the partial volatilization of chemical that had been adsorbed to the bubble surface. Incidentally, none of the described processes affects the performance of the PRV−HS method. As discussed in the theory section, unless sorption to the glass wall and the air−water interface is very strong, it should not appreciably affect the phase distribution between gas and aqueous phase in a closed headspace vial. Also, evaporative losses from the water phase are not relevant in a closed system. In light of the findings of the present study, we suggest that it would be appropriate to evaluate the air−water partitioning data that have been generated for substances with relatively high K_{IA} using the IGS method.

Literature Cited

(1) Schwarzenbach, R. P.; Gschwend, P. M.; Imboden, D. M. *Environmental Organic Chemistry*; John Wiley & Sons: New York, 1993.

(2) Leroi, J.-C.; Masson, J.-C.; Renon, H.; Fabries, J.-F.; Sannier, H. Accurate measurements of activity coefficients at infinite dilution by inert gas stripping and gas chromatography. *Ind. Eng. Chem., Process Des. Dev.* **1977**, *16*, 139−144.

(3) Mackay, D.; Shiu, W. Y.; Sutherland, R. P. Determination of air−water Henry's law constants for hydrophobic pollutants. *Environ. Sci. Technol.* **1979**, *13*, 333−337.

(4) Alaee, M.; Whittal, R. M.; Strachan, W. M. J. The effect of water temperature and composition on Henry's law constant for various PAHs. *Chemosphere* **1996**, *32*, 1153−1164.

(5) Hovorka, Š.; Dohnal, V. Determination of air−water partitioning of volatile halogenated hydrocarbons by the inert gas stripping method. *J. Chem. Eng. Data* **1997**, *42*, 924−933.

(6) Ten Hulscher, T. E. M.; Van Der Velde, L. E.; Bruggeman, W. A. Temperature dependence of Henry's law constants for selected chlorobenzenes, polychlorinated biphenyls and polycyclic aromatic hydrocarbons. *Environ. Toxicol. Chem.* **1992**, *11*, 1595−1603.

(7) Shiu, W. Y.; Mackay, D. Henry's law constants of selected aromatic hydrocarbons, alcohols, and ketones. *J. Chem. Eng. Data* **1997**, *42*, 27−30.

(8) De Maagd, P. G.-J.; ten Hulscher, T. E. M.; van den Heuvel, H.; Opperhuizen, A.; Sijm, D. T. H. M. Physicochemical properties of polycyclic aromatic hydrocarbons: aqueous solubilities, *n*-octanol/water partition coefficients, and Henry's law constants. *Environ. Toxicol. Chem.* **1998**, *17*, 251−257.

(9) Bamford, H. A.; Poster, D. L.; Baker J. E. Method for measuring the temperature dependence of the Henry's law constant of selected polycyclic aromatic hydrocarbons. *Polycyclic Aromat. Compd.* **1999**, *14*/*15*, 11−22.

(10) Bamford, H. A.; Poster, D. L.; Baker, J. E. Temperature dependence of Henry's law constants of thirteen polycyclic aromatic hydrocarbons between 4 and 31 °C. *Environ. Toxicol. Chem.* **1999**, *18*, 1905−1912.

(11) Ten Hulscher, T. E. M.; van den Heuvel, H.; van Noort, P. C. M.; Govers, H. A. J. Henry's law constants for eleven polychlorinated biphenyls at 20 °C. *J. Chem. Eng. Data* **2006**, *51*, 347 -351.

(12) Bamford, H. A.; Poster, D. L.; Baker, J. E. Henry's law constants of polychlorinated biphenyl congeners and their variation with temperature. *J. Chem. Eng. Data* **2000**, *45*, 1069−1074.

(13) Lau, F. K.; Charles, M. J.; Cahill, T. M. Evaluation of gas-stripping methods for the determination of Henry's law constants for polybrominated diphenyl ethers and polychlorinated biphenyls. *J. Chem. Eng. Data* **2006**, *51*, 871−878.

(14) Cetin, B.; Odabasi, M. Measurement of Henry's law constants of seven polybrominated diphenyl ether (PBDE) congeners as a function of temperature. *Atmos. Environ.* **2005**, *39*, 5273−5280.

(15) Odabasi, M.; Cetin, B.; Sofuoglu, A. Henry's law constant, octanol−air partition coefficient and supercooled liquid vapor pressure of carbazole as a function of temperature: application to gas/particle partitioning in the atmosphere. *Chemosphere* **2006**, *62*, 1087−1096.

(16) Kucklick, J. R.; Hinckley, D. A.; Bidleman, T. F. Determination of Henry's law constants for hexachlorocyclohexanes in distilled water and artificial seawater as a function of temperature. *Mar. Chem.* **1991**, *34*, 197−209.

(17) Sahsuvar, L.; Helm, P. A.; Jantunen, L. M. M.; Bidleman, T. F. Henry's law constants for α-, *β*-, and *γ*-hexachlorocyclohexanes (HCHs) as a function of temperature and revised estimates of gas exchange in Arctic regions. *Atmos. Environ.* **2003**, *37*, 983−992.

(18) Jantunen, L. M. M.; Bidleman, T. F. Temperature dependent Henry's law constant for technical toxaphene. *Chemosphere: Global Change Sci.* **2000**, *2*, 225−231.

(19) Cetin, B.; Ozer, S.; Sofuoglu, A.; Odabasi, M. Determination of Henry's law constants of organochlorine pesticides in deionized and saline water as a function of temperature. *Atmos. Environ.* **2006**, *40*, 4538−4546.

(20) Jantunen, L. M. M.; Bidleman, T. F. Henry's law constants for hexachlorobenzene, *p*,*p*′-DDE and components of technical chlordane and estimates of gas exchange for Lake Ontario. *Chemosphere* **2006**, *62*, 1689−1696.

(21) Goss, K.-U.; Wania, F.; McLachlan, M. S.; Mackay, D.; Schwarzenbach, R. P. Comment on "Re-evaluation of air−water exchange fluxes of PCBs in Green Bay and Southern Lake Michigan". *Environ. Sci. Technol.* **2004**, *38*, 1626−1628.

(22) Baker, J. E.; Totten, L. A.; Gigliotti, C. L.; Offenberg, J. H.; Eisenreich, S. J.; Bamford, H. A.; Huie, R. E.; Poster, D. L. Response to comment on "Reevaluation of air−water exchange fluxes of PCBs in Green Bay and Southern Lake Michigan". *Environ. Sci. Technol.* **2004**, *38*, 1629−1632.

(23) Sagebiel, J. C.; Seiber, J. N.; Woodrow, J. E. Comparison of headspace and gas-stripping methods for determining the Henry's law constant (*H*) for organic compounds of low to intermediate H. *Chemosphere* **1992**, *12*, 1763−1768.

(24) Hartkopf, A.; Karger, B. L. Study of the interfacial properties of water by gas chromatography. *Acc. Chem. Res.* **1973**, *6*, 209−216.

(25) Hoff, J. T.; Mackay, D.; Gillham, R.; Shiu, W. Y. Partitioning of organic chemicals at the air-water interface in environmental systems. *Environ. Sci. Technol.* **1993**, *27*, 2174−2180.

(26) Ettre, L. S.; Kolb, B. Headspace-gas chromatography: the influence of sample volume on analytical results. *Chromatographia* **1991**, *32*, 5−12.

(27) Ettre, L. S.; Welter, C.; Kolb, B. Determination of gas−liquid partition coefficients by automatic equilibrium headspace−gas chromatography utilizing the phase ratio variation method. *Chromatographia* **1993**, *35*, 73−84.

(28) Lei, Y. D.; Wania, F.; Mathers, D.; Mabury, S. A. Determination of vapor pressures, octanol−air and water−air partition coefficients for

polyfluorinated sulfonamid, sulfonamidoethanols and telomer alcohols. *J. Chem. Eng. Data* **2004**, *49*, 1013−1022.
(29) Goss, K. U. Prediction of the temperature dependency of Henry's law constant using poly-parameter linear free energy relationships. *Chemosphere* **2006**, *42*, 1369−1374.
(30) Roth, C. M.; Goss, K.-U.; Schwarzenbach, R. P. Adsorption of a diverse set of organic vapors on the bulk water surface. *J. Colloid Interface Sci.* **2002**, *252*, 21−30.
(31) Roth, C. M.; Goss, K.-U.; Schwarzenbach, R. P. Sorption of diverse organic vapors to snow. *Environ. Sci. Technol.* **2004**, *38*, 4078−4084.
(32) Costanza, M. S.; Brusseau, M. L. Contaminant vapor adsorption at the gas-water interface in soils. *Environ. Sci. Technol.* **2000**, *34*, 1−11.
(33) Kelly, C. P.; Cramer, C. J.; Truhlar, D. G. Predicting adsorption coefficients at air-water interfaces using universal solvation and surface area models. *J. Phys. Chem. B* **2004**, *108*, 12882−12897.
(34) Goss, K. U. Predicting the equilibrium partitioning of organic compounds using just one solvation energy relationship (LSER). *Fluid Phase Equilib.* **2005**, *233*, 19−22.
(35) Xiao, H.; Lei, Y. D.; Wania, F. Determination of partitioning coefficients of numerous organic solutes between a long chain aliphatic alcohol and the gas phase as a function of temperature. *J. Chem. Eng. Data* **2006**, *51*, 338−346.
(36) Kolb, B.; Welter, C.; Bichler, C. Determination of partition coefficients by automatic equilibrium headspace gas chromatography by vapor phase calibration. *Chromatographia* **1992**, *34*, 235−240.
(37) Vrbka, P.; Fenclová, D.; Laštovka, V.; Dohnal, V. Measurements of infinite dilution activity coefficients of 1-alkanols (C1 to C5) in water as a function of temperature (273−373 K). *Fluid Phase Equilib.* **2005**, *237*, 123−129.
(38) Gupta, A. K.; Teja, A. S.; Chai, X. S.; Zhu, J. Y. Henry's constants of *n*-alkanols (methanol through *n*-hexanol) in water at temperatures between 40 °C and 90 °C. *Fluid Phase Equilib.* **2000**, *170*, 183−192.
(39) Butler, J. A. V.; Ramchandani, C. N., Thomson, D. W. The solubility of non-electrolytes. Part I. The free energy of hydration of some aliphatic alcohols. *J. Chem. Soc.* **1935**, *952*, 280−285.
(40) Burnett, M. G. Determination of partition coefficients at inifinite dilution by the the gas chromatographic analysis of the vapor above dilute solutions. *Anal. Chem.* **1963**, *35*, 1567−1570.
(41) Snider, J. R.; Dawson, G. A. Troposheric light alcohols, carbonyls, and acetonitrile: concentrations in the southwestern United States and Henry's law data. *J. Geophys. Res.* **1985**, *90*, 3797−3805.
(42) Buttery, R. G.; Ling, L. C.; Guadagni, D. G. Food volatiles. Volatilities of aldehydes, ketones, and esters in dilute water solution. *J. Agric. Food Chem.* **1969**, *17*, 385−389.
(43) Mackay, D.; Shiu, W. Y.; Ma, K. C.; Lee, S. C. *Handbook of Physical-Chemical Properties and Environmental Fate for Organic Chemicals. Vol. III Oxygen Containing Compounds*, 2nd ed.; CRC Press: Boca Raton, FL, 2006.

Received for review August 1, 2006. Accepted October 12, 2006. We are grateful for financial support from the Natural Sciences and Engineering Research Council of Canada.

JE060344Q